Received: 15 November 2020 | Accepted: 27 November 2020

DOI: 10.1002/maco.202012191

ARTICLE

Materials and Corrosion

Preconditioning of AISI 304 stainless steel surfaces in the presence of flavins—Part I: Effect on surface chemistry and corrosion behavior

Nina Wurzler | Oded Sobol | Korinna Altmann | Jörg Radnik | Ozlem Ozcan

Bundesanstalt für Materialforschung und -prüfung, Berlin, Germany

Correspondence
Ozlem Ozcan, Bundesanstalt für Materialforschung und -prüfung, Unter den Eichen 87, 12205 Berlin, Germany.
Email: ozlem.ozcan@bam.de

Abstract

Stainless steel AISI 304 surfaces were studied after a mild anodic polarization for oxide growth in the presence and absence of two derivatives of vitamin B2 (riboflavin and flavin mononucleotide) that can be secreted by metal-reducing bacteria and act as a chelating agent for iron species. The alterations in oxide chemistry were studied by means of surface-sensitive techniques such as X-ray photoelectron spectroscopy and time-of-flight secondary ion mass spectrometry analysis. The complementary electrochemical characterization revealed a preferential growth of an oxide/hydroxide iron-rich film that is responsible for an altered pit initiation and nucleation behavior. These findings suggest that as the corrosion behavior is determined by the interplay of the chemical and electronic properties, only a mild anodic polarization in the presence of redox-active molecules is able to alter the chemical and electronic structure of the passive film formed on stainless steel AISI 304. This helps to achieve a profound understanding of the mechanisms of microbially influenced corrosion (MIC) and especially the possible effects of the redox-active biomolecules, as they may play an important role in the corrosion susceptibility of stainless steel surfaces.

KEYWORDS

corrosion, flavins, passive film chemistry, stainless steel, surface analysis

1 | INTRODUCTION

The outstanding corrosion properties of stainless steels are due to the formation of a 1–3 nm thin passive film, which consists of mainly iron and chromium oxides and hydroxides.[1,2] These surface oxides are distinct in their chemical composition and electrochemical behavior, and are therefore responsible for the passivation of the steel and its corrosion resistance. Among the electrochemical properties, semiconducting characteristics play an important role in the growth and stability of passive films in different environments. Passive films formed at neutral pH are reported to be structured as a bilayer with an n-type iron oxyhydroxide-rich outer layer and a p-type chromium oxyhydroxide-rich inner layer.[3–5] The dopant or charge carrier density determines the protective properties of the passive film.

Despite the high corrosion resistance of stainless steels, the structure and chemistry of the protective passive film can be altered due to microbial activity and lead to microbially influenced corrosion (MIC). In a recent study, Zhang et al. demonstrated that the addition of electron shuttle molecules excreted by *Shewanella* spp. significantly accelerates MIC of 304 stainless steel by *Desulfovibrio vulgaris*, a sulfate-reducing bacteria. According to Zhang et al.,[6] the addition of electron shuttle molecules at the ppm level has resulted in a doubling of the mass loss and an increase in the pit depths.

Shewanella putrefaciens belong to the group of electroactive bacteria. This specific type is capable of dissimilatory electron transfer to various metals as electron acceptors.[7–11] There are different proposed modes for the electron transfer processes of *Shewanella* spp., including the direct contact of cell extensions and the cell's outer membrane *c*-type cytochromes or by utilizing the conducting minerals such as humic acids in the biofilm and the environment.[12–14] However, as reported by Marsili et al.[7] in his pioneering publication, the most dominant mode of electron transfer is the secretion and utilization of redox molecules, the so-called electron shuttles, which can overcome large distances by diffusion through the biofilm to the substrate surface. Riboflavin (RB) and its derivative flavin mononucleotide (FMN)[15] are assumed to be the redox center of microorganisms' flavoenzymes[16] and have a common electroactive moiety. This isoalloxazine group can be present in three different protonation states and, therefore, store and release electrons.[17] Moreover, flavin molecules are known to be able to act as chelating agents for iron passivation layers and to catalyze the cathodic oxygen reduction reaction.[7,18] According to the literature, *Shewanella* spp. start producing and secreting flavins after 1–2 days after the settlement on surfaces where the concentration of these redox molecules is predicted to stabilize approximately at 1–2 μM in the biofilm.[19]

Due to their adaptability, passive films on stainless steels have the ability of dynamically changing in response to their environment. Thus, for a profound understanding of the interaction mechanisms of microbes with stainless steel surfaces, it is essential to understand the changes in the chemical composition, dissolution, and corrosion behavior as well as electrical properties of passive films in different common environments. Besides facilitating electron transfer between the microorganisms and the stainless-steel substrate, the presence of flavins could also influence the passive film chemistry.

The goal of the present work is to investigate the influence of the presence of *Shewanella's* electron shuttle molecules during short duration, mild anodic polarization (+50 mV vs. open-circuit potential [OCP]). The results shall help in interpreting the electrochemical interaction of bacteria with steels, especially in discussing the indirect role of electron shuttle molecules affecting the corrosion behavior of microbial consortia.

TABLE 1 Chemical composition of the alloy AISI 304 (measured with inductively coupled plasma optical emission spectrometry)

AISI 304	Mn	Cr	Ni	C	S, N, Si, P
wt%	0.97	18.52	8.02	0.035	≪1

2 | MATERIALS AND METHODS

2.1 | Sample preparation

For the purpose of this study, austenitic stainless steel sheets of type AISI 304 (1.4301) with a chemical composition as listed in Table 1 were chosen. The steel was received in the fully annealed condition, as a 1.2-mm-thick sheet. The samples were cut into coupons (1.5 × 1.5 cm) and mechanically polished with silicon carbide polishing paper up to 600 grit (P1200). The surface was rinsed and cleaned with acetone in an ultrasonic bath for 10 min.

A noninteracting $NaClO_4$ electrolyte and a low-amplitude/short-duration potentiostatic polarization were selected for the polarization step to minimize artifacts and to focus the study on the effect of flavin molecules.[20] The artifacts might occur due to the incorporation of electrolyte anions like chlorides or sulfates into the passive film. The steel coupons were preconditioned potentiostatically for 1 h at +50 mV versus OCP (three-electrode setup with gold-wire counter electrode and sat. Ag/AgCl reference electrode, Gamry 600+ potentiostat; C3 Prozessanalytik) in a solution containing 20-mM $NaClO_4$ and 1-μM riboflavin (>98% purity; Sigma-Aldrich) or flavin mononucleotide (73%–79% fluorometric; Sigma-Aldrich). It should be noted that these samples will be referred to as RB and FMN later on. As a control sample, one coupon was preconditioned in 0.02-M $NaClO_4$ only, under the same conditions (pure). Unless the purity is specifically declared, all solutions were prepared using analytical grade solvents and deionized water (0.055 μS/cm; Evoqua).

2.2 | Characterization of surface chemistry

X-ray photoelectron spectroscopy (XPS) measurements were performed on a SAGE 100 spectrometer (Specs) under ultrahigh vacuum with pressure lower than 1×10^{-7} mbar. The photoelectrons were excited by nonmonochromatic Al

Kα radiation with an energy of 1486.6 eV. The angle between X-ray source and analyzer was 54.9°. The analyzer was 18° to the surface normal. Spectra were acquired at 10-kV, 18-mA, and 20-eV pass energy in the constant analyzer energy mode. At least three replicates on each of the three independent samples were analyzed with a spot size of $1 \times 3\ mm^2$ before calculating a mean value, which is presented in the following. All binding energies were referenced to the C 1s peak of aliphatic hydrocarbon at 284.9 eV. Spectra fitting was performed using CasaXPS analysis software (version 2.3.15). For quantitative analysis, Shirley background function and a Gaussian/Lorentzian product function peak shape model GL(30) were used for all peaks except the metal peaks. For iron and chromium metal peaks, an asymmetric tail was considered using GL (50)T2 line shapes. The uncertainty in the determination of the electron binding energy is ±0.2 eV.

Time-of-flight secondary ion mass spectrometry (ToF-SIMS) measurements were performed on a ToF-SIMS IV instrument (IONTOF) using 25-kV Bi^{1+} primary ions. The analyses were conducted at a pressure of 10^{-9} mbar in the spectrometry mode of the instrument (i.e., high-current bunched mode) with a field of view of $100 \times 100\ \mu m^2$. Elemental and molecular information from the analyzed sample surface were acquired by setting the detector in the negative polarity (allowing a better sensitivity to O- and OH-containing fragments). Sequential sputtering was performed using a 1-kV Cs + sputter beam with a sputter area of $300 \times 300\ \mu m^2$, allowing to perform depth profile and to enhance the negative secondary ion yield (e.g., oxides). The analyzed region was set at the center of the sputtered region. Data acquisition and post-processing were performed using IONTOF SurfaceLab 6.8. To determine the surface composition, the following peaks have been selected: (1) FeO^- ($m/z = 72$), (2) FeO_2^- ($m/z = 88$), (3) $FeOH^-$ ($m/z = 73$), (4) CrO^- ($m/z = 68$), (5) CrO_2^- ($m/z = 84$), (6) $CrOH^-$ ($m/z = 69$), (7) O_2^- ($m/z = 84$), (8) OH^- ($m/z = 17$), and (9) CN^- ($m/z = 26$). For the analyses and the discussion, layer thickness was determined on the basis of the time span between half intensity $t_{1/2}$ and $t_{-1/2}$ (in the increasing and decreasing directions, respectively). All depth profiles were repeated five times for each preconditioning system.

2.3 | Electrochemical characterization and corrosion studies

The semiconducting properties of the passive films were investigated by means of Mott–Schottky analysis based on capacitance values determined from electrochemical impedance spectra (EIS). These values were collected in a potential range of ±0.4 V versus OCP of the prepared substrates. A saturated calomel reference electrode (ALS Co. Ltd. BAS Japan) and a gold wire served as reference and counter electrodes, respectively. Propylene carbonate-containing 0.1-M $NaClO_4$ solution was used as an electrolyte to suppress corrosion processes, which result in changes in the passive film chemistry at anodic potentials and minimize electrical double-layer effects.[21,22] EIS spectra were collected in a frequency range of 100 MHz–1 Hz with an applied AC potential of 10 mV and a potential step size of 50 mV. The data were fitted using an equivalent circuit composed of the electrolyte resistance (R_{El}) in series with the parallel combination of the space charge capacitance and the charge transfer resistance (R_{CT}). The space charge capacitance (C_{sc}) was represented with a constant phase element (CPE: Y_{SC}, α_{SC}) to compensate for the inhomogeneities in the passive film structure. The capacitance value was calculated from the CPE fit parameters according to Equation (1), where the f_{max} is the value at which the minimum phase angle was observed in the investigated frequency range:

$$C_{SC} = Y_{SC}(f_{max})^{\alpha_{SC}-1}. \quad (1)$$

The calculations of the donor densities (N_D) and flat band potential (V_{fb}) were performed according to Equation (2) for the capacitance behavior of an n-type semiconductor, where ε_0 (vacuum permittivity) $= 8.85 \times 10^{-14}$ F/cm, q (elementary charge) $= 1.602 \times 10^{-19}$ C and ε is the dielectric constant of the passive film and is taken as 40.[23]

$$\frac{1}{C_{SC}^2} = \frac{2}{\varepsilon\varepsilon_0 N_D A^2}\left(V - V_{fb} - \frac{kT}{q}\right). \quad (2)$$

The film thickness of the dielectric layer, d_{sc}, can be calculated using the following equation:

$$d_{sc} = \frac{\varepsilon\varepsilon_0}{C_{sc}}, \quad (3)$$

where C_{sc} is the area-corrected capacitance data.[24]

For the investigation of localized corrosion cyclic polarization, measurements were performed between −0.3 and +1 V versus OCP with a current cut-off at 25 μA and a sweep rate of 1 mV/s. After the current cut-off was reached, the potential was cycled back with the same rate to the OCP value to study the repassivation behavior. A 500-mM NaCl solution was used as an electrolyte after de-aeration via bubbling with high-purity nitrogen for 60 min. After pitting experiments, the coupons were taken out of the electrochemical cell, rinsed with acetone, and cleaned in an

ultrasonic bath with a solution containing 1 M of oxalic acid (98%; Sigma-Aldrich) for 10 min to remove the corrosion products. The scanning electron microscopy (SEM) analysis was carried out on a Zeiss SEM Evo MA10 in the SE mode at 7×10^{-5} mbar vacuum (Zeiss). All electrochemical tests were carried out at least in triplicate from independent samples.

3 | RESULTS

3.1 | Corrosion properties

The aim of this study was to clarify whether the presence of minute amounts of redox-active flavin molecules in the environment can alter the passive film chemistry. The electrochemical investigations were carried out after a short-duration (60 min), small-magnitude (+50 mV vs. OCP) anodic polarization in the presence or absence of flavin molecules. To assess the corrosion properties, cyclic polarization tests have been conducted, and the resulting current density/potential curves are presented in Figure 1.

The first clear effect observed in the cyclic polarization results is the slight decrease in pitting potential for surfaces that are preconditioned in the presence of 1-μM FMN. For these samples, the onset of pitting was below 100 mV and the current cut-off was reached already at ~190 mV. According to the results of the cyclic polarization experiments, the addition of RB did not result in a significant change in the pitting susceptibility in comparison to the samples preconditioned without any flavins. The second important effect was that, under these experimental conditions, only the surfaces preconditioned in the presence of FMN have shown repassivation. For these samples, the hysteresis was also considerably lower than for the other two systems. During the late phases of the cathodic sweep after the sudden current drop, pure and RB samples have still shown a nearly steady current density of 2.1 and 3.5 $\mu A/cm^2$, respectively. The anodic-to-cathodic transition was observed for pure and RB samples below the corrosion potential.

After cyclic polarization experiments, the extent of pitting was analyzed by means of SEM. As seen in the SEM micrographs of pure, FMN, and RB samples presented in Figure 2, another clear difference was observed in their pitting behavior. The samples preconditioned in the flavin-containing electrolytes exhibited a smaller number of pits in comparison to the samples preconditioned in the absence of the flavin molecules. This observation indicates an improvement in the susceptibility of the passive film to pit nucleation. However, the addition of RB, as well as FMN, resulted in larger and deeper

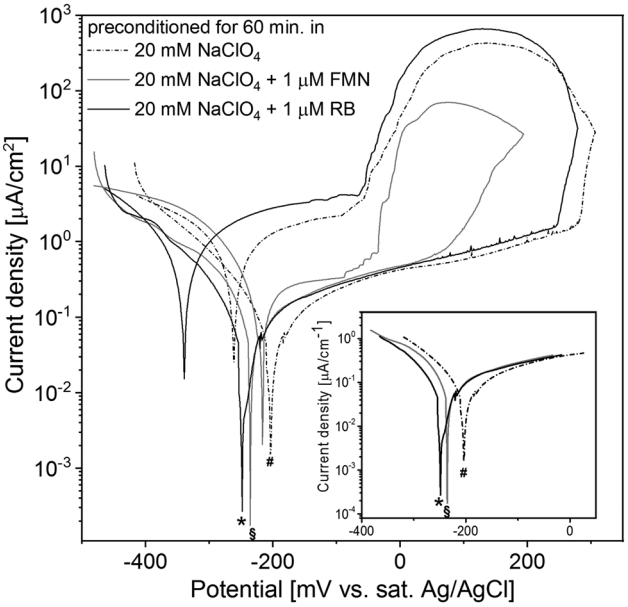

FIGURE 1 The representative current density versus potential curves of AISI 304 stainless steel surfaces in 500-mM NaCl electrolyte (inset: Tafel region)

pits. The selection of a low current cut-off enabled the probing of the passive layer stability and the repassivation behavior of the samples, without causing an extensive corrosive attack.

3.2 | Differences in the passive film chemistry

To gain a deeper insight into these differences, surface analytical measurements by means of ToF-SIMS and XPS have been performed. The elemental composition of the passive film was studied by the analysis of the XPS detail spectra of major constituents: Fe (2p 3/2), Cr (2p 3/2), O (1s), and C (1s). As listed in Table 2, the presence of flavin molecules has resulted in a slightly higher iron content and higher Fe/Cr ratio in the passive film when compared with the samples preconditioned without the addition of flavins. Considering the different pit nucleation and growth behavior, ToF-SIMS sputter profiles were acquired on all three systems. A detailed analysis has been performed to distinguish different oxide and hydroxide peaks. The FeO_2^-, CrO_2^-, $FeOH^-$, and $CrOH^-$ signals have been selected to describe the passive film structure due to their high intensities and signal-to-noise ratio. The analysis of other relevant negatively charged signals such as FeO^-, CrO^-, O_2^-, and OH^-, as well as the neutral oxide signals Fe_2O_3 and Cr_2O_3, which have relatively low counts, did not change the main conclusions regarding the layer structure. In the results and

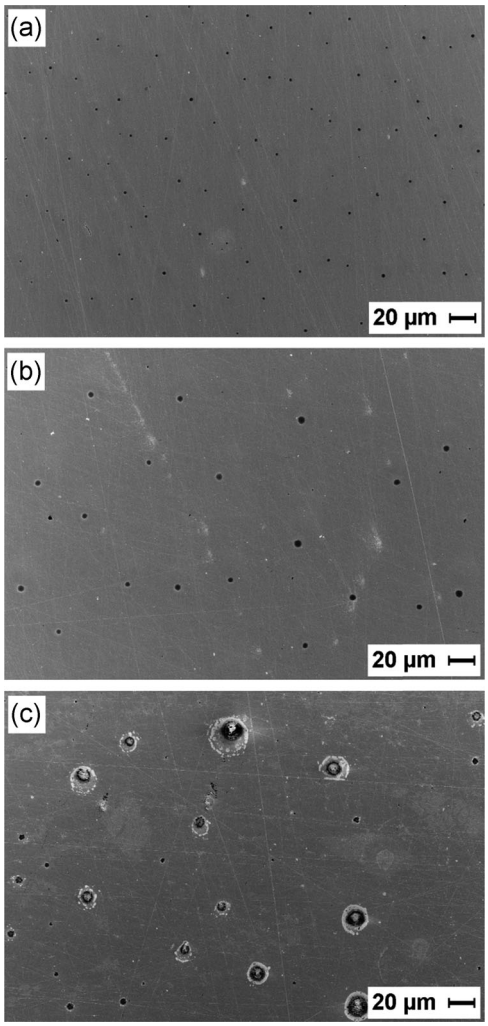

FIGURE 2 Scanning electron microscopy images of the (a) pure, (b) flavin mononucleotide, and (c) riboflavin samples after the cyclic polarization experiments

discussion sections, we refer to sputter times rather than the sputter rates due to the complexity to determine the layer thickness.

The ToF-SIMS profiles of FeO_2^-, CrO_2^-, $FeOH^-$, and $CrOH^-$ signals are presented in Figure 3a,b, together with the times at half maximum intensity values for each fragment and each sample set in Figure 3c. The beginning and end of the specific signal are represented by a number indicating the sputter time in seconds and a grayscaled bar for better visibility. The presence of flavins during the polarization step leads to thicker passive films. In all samples, the fragments that were detected at first

TABLE 2 The XPS elemental composition of the passive film in at%, considering only Fe, Cr, O, C, and the resulting Fe/Cr ratio

(At%)	Fe	Cr	O	C	Fe/Cr
Pure	10.5	7.4	55.7	26.5	1.42
FMN	12.0	6.7	55.1	26.3	1.79
RB	12.4	7.5	53.6	26.5	1.65

Abbreviations: FMN, flavin mononucleotide; RB, riboflavin; XPS, X-ray photoelectron spectroscopy.

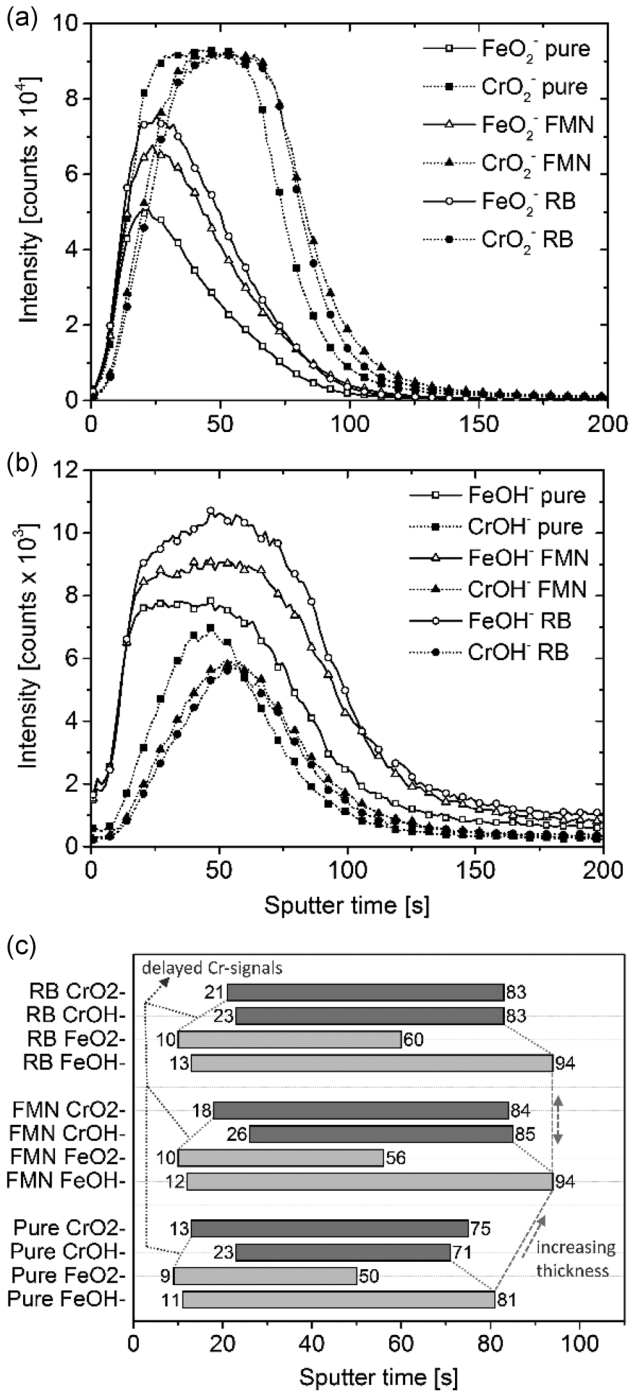

FIGURE 3 Time-of-flight secondary ion mass spectrometry sputter depth profiles of (a) oxides (FeO_2^- (m/z: 88), CrO_2^- (m/z: 84)) and (b) hydroxides ($FeOH^-$ (m/z: 73), $CrOH^-$ (m/z: 69)) signals; (c) the summary of the time-at-half-max-intensity values for all species and samples. FMN, flavin mononucleotide; RB, riboflavin

were FeO_2^- and $FeOH^-$. In the case of the pure sample, the CrO_2^- signal appears early after 4 s of sputtering time, in comparison to FMN (8 s) and RB (11 s), indicating the coexistence of both Fe and Cr oxides throughout the oxide film. Overall, considering the first and last signals of each system set, the ToF-SIMS data indicate that the passive film on the FMN and RB is of similar thickness and ~17% thicker than the one on the pure sample.

Although a direct determination of the concentration of certain metal hydroxide and oxide species is not possible by means of ToF-SIMS, the trends and the ratios of maximum counts could still be used for a qualitative description. As seen in Figure 3a, the highest FeO_2^-/CrO_2^- and $FeOH^-/CrOH^-$ ratios were measured for RB as 0.8 and 1.88, respectively, followed by 0.71 and 1.52 for FMN, and 0.54 and 1.15 for the pure samples (highest intensity at plateau region; Figure 3a,b). Only on the RB sample, the CrO_2^- and $CrOH^-$ signals appear nearly at the same time in the sputter profiles. For the other two, the signal of the $CrOH^-$ was detected with an additional 8–10 s of delay.

On the basis of the layer model derived from ToF-SIMS results, the analysis of the XPS spectra has been performed according to Devito and Marcus.[25] The fitting of Fe 2p 3/2 peak was performed by considering metallic iron (Fe^0: 706.7 eV), ferrous (Fe^{2+}: 709.7 eV), and ferric (Fe^{3+}: 711.5 eV) oxide and hydroxide species (spectra presented in Supporting Information). For the Cr 2p 3/2 peak, metallic chromium (Cr^0: 773.6 eV), trivalent chromium oxides (Cr^{3+}: 576.1 eV), and hydroxides ($Cr^{3+}OH$: 577.1 eV) were evaluated. The O 1s spectra were fitted with the contributions of metal oxides (O^{2-}: 529.4 eV), hydroxides (OH: 530.9 eV), and oxygen from organic contaminations as well as water incorporated into the passive film (C═O, POOH, H_2O: 532.3 eV). The spectra with component fitting are presented in the Supporting Information.

The results of the XPS component analysis of Fe 2p 2/3 and Cr 2p 2/3 spectra are presented in Figure 4. The XPS analysis clearly indicates that the amount of metallic iron and ferric oxides and hydroxides remains almost constant, and the ferrous oxide increases from 2.9 at% (pure) to 4.5 at% (FMN) and 4.9 at% (RB) with the presence of the electron shuttle molecules during the preconditioning step. The metallic Cr content of the passive film is slightly decreased for both flavin systems, which can be explained by the presence of a thicker oxide film. Moreover, the trivalent Cr oxide concentration is slightly lower for FMN and slightly higher for the RB sample in comparison to the pure surfaces. The amount of trivalent Cr hydroxides was comparable on all three sample sets.

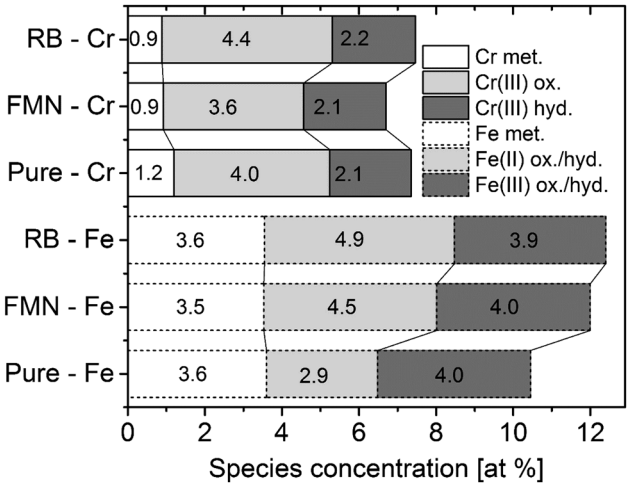

FIGURE 4 Atomic percentages of components obtained from the analysis of Fe 2p 3/2 and Cr 2p 3/2 detail spectra. FMN, flavin mononucleotide; RB, riboflavin

The distribution of the components in the O 1s spectra is presented in Figure 5. A higher concentration of oxidic species was observed on passive films preconditioned in solutions containing flavin molecules in comparison to samples preconditioned in only $NaClO_4$ medium. The contribution from H_2O and organic compounds was slightly lower for FMN and RB samples. The samples preconditioned in the presence of RB had a lower hydroxide content in the passive film.

The Mott–Schottky analysis has been performed to analyze the semiconducting behavior of the passive films formed in different solutions. The approximation of dielectric constants for the bilayer system leads to an uncertainty in the values calculated for donor densities and thickness values. The high sensitivity of these constants to the crystalline structure is responsible for the imperfection of the applied equations and models.[23] In this study, the Mott–Schottky analysis is intended to achieve an approximation of semiconducting properties to help interpret the results of surface characterization.

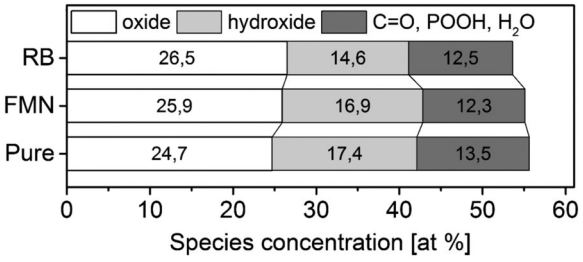

FIGURE 5 Atomic percentages of components obtained from the analysis of O 1s detail spectra in relation to overall oxygen at%. FMN, flavin mononucleotide; RB, riboflavin

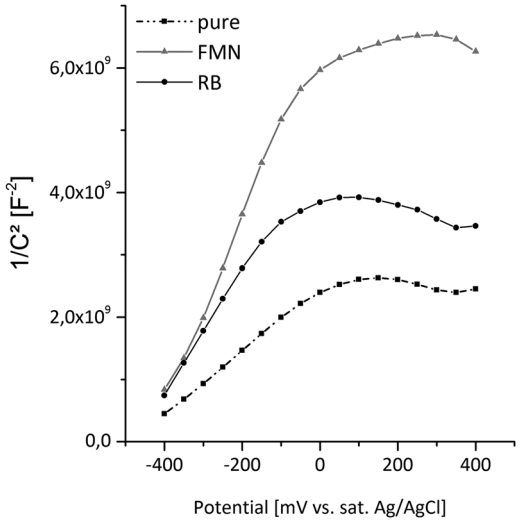

FIGURE 6 Mott–Schottky plots calculated from impedance measurements at frequencies ranging from 100 MHz to 1 Hz. FMN, flavin mononucleotide; RB, riboflavin

The region with a linear relationship between $1/C^2$ and E in Equation (2) (−400 to 0 mV vs. Ag/AgCl) shows positive slopes, which are attributed to an n-type behavior in the selected potential range. The donor densities from the linear range in Figure 6 are calculated according to Equation (2) and presented in Table 3. The highest donor density was observed with the pure sample, followed by RB and FMN, with values of 5.5×10^{20}, 2.8×10^{20}, and $2.2 \times 10^{20}\,\mathrm{cm}^{-3}$, respectively. The calculated film thicknesses (Equation 3) ranging from 1.95 to 2.71 nm are in good agreement with the literature values reported on iron[24] and stainless steels.[26]

According to Hakiki et al.[26] and Fattah-Alhosseini & Khalvan,[27] the n-type character is promoted by the presence of FeO compounds and the inner layer is dominated by chromium species; therefore, it is characterized by a p-type behavior. The higher donor density for pure samples could be explained by the nonstoichiometric space charge region arising from the iron–chromium mixtures.[26] In general, structural lattice defects decrease with an increase in the film thickness, resulting in a lower conductivity.[24] The Mott–Schottky behavior is a response of the amorphous nature of the oxide layer, which can also be influenced by chemisorbed species.[26] As shown in Figure 7, a high CN^- signal was observed with films preconditioned in the presence of FMN in comparison to the RB and pure samples. This could indicate an incorporation or adsorption of FMN molecules in/on the passive layer surface, which could lead to an increased anion density influencing the Helmholtz layer and therefore contribute to pseudo-capacitance.[28]

TABLE 3 The Mott–Schottky analysis: donor densities (N_D) obtained from slopes in Figure 6 and passive layer thicknesses calculated from d_{sc} in Equation (3)

	Pure	FMN	RB
N_D ($\times 10^{20}\,\mathrm{cm}^{-3}$)	5.50	2.17	2.82
V_{fb}	−4,89E-01	−4,80E-01	−5,02E-01
d (nm)	1.96	2.71	2.55

Abbreviations: FMN, flavin mononucleotide; RB, riboflavin.

4 | DISCUSSION

Combining the results of the XPS and ToF-SIMS analyses, a clear description of the passive layer chemistry and structure can be drawn. The most significant differences observed in terms of the chemical composition were the higher ratio of ferrous components as well as a higher concentration of oxidic species on the FMN and RB samples in comparison to samples preconditioned in the absence of flavins. Moreover, based on the ToF-SIMS results, the layered structure of the passive film became more prominent for FMN and RB samples. The preconditioning in the presence of flavin molecules resulted in a nearly pure iron oxide layer at the outermost surface of the passive film. The lower passive film thickness calculated for the samples preconditioned without the addition of flavin molecules agrees well with the highest metal-to-oxide ratio observed in the XPS analysis and with the lower ToF-SIMS sputtering time in comparison to the samples preconditioned in the presence of flavins.

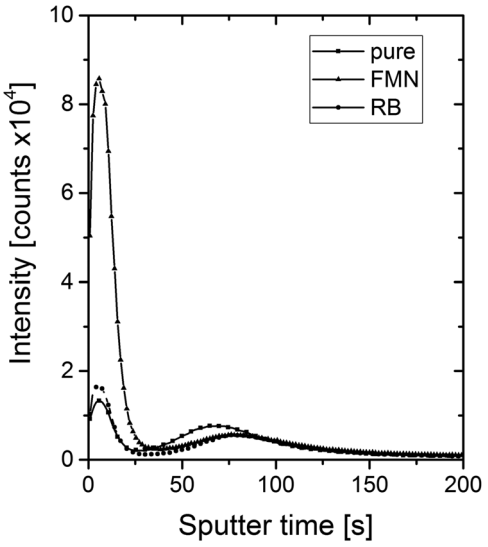

FIGURE 7 Time-of-flight secondary ion mass spectrometry sputter depth profiles of CN signal. FMN, flavin mononucleotide; RB, riboflavin

Comparing the FMN and RB samples, the passive film thickness is very similar. From the increase in the oxide layer thickness of the samples preconditioned in the presence of flavins, a higher resistance to pitting corrosion was expected. On the contrary, FMN and RB have shown different susceptibilities to pitting corrosion. Among all three systems, FMN is the one that indicates a depletion of chromium oxides in the passive film, which can explain the occurrence of an early onset of pitting corrosion. The most significant influence of flavins was the increase of the resistance to pit nucleation. Samples preconditioned in the presence of flavins had very few but larger pits after the cyclic polarization experiments in comparison to samples preconditioned in the absence of flavin molecules. The lower donor densities estimated from the Mott–Schottky analysis, together with the increase in the iron oxide-dominated outer layer of the passive film, can explain the observed changes in the pitting behavior. Especially for the RB samples, the elevated amount of iron oxides could have led to a suppression of the onset of pitting corrosion to a certain degree. However, exceeding the activation energy, the pitting occurs in the form of large pits and results in high corrosion current densities once the pit nucleation is initiated.[29]

5 | CONCLUSIONS

Our results demonstrate that only the presence of redox-active flavin molecules during a mild anodic polarization of short duration can alter the chemical and electronic structure of the passive film formed on stainless steel AISI 304. As a result, significant changes in the corrosion behavior are induced. The preconditioning in the presence of flavin molecules led to a preferential growth of Fe(II)-rich outer layers during passive film growth. In the case of FMN, the lower concentration of chromium species and the presence of adsorbed FMN on the surface lowered the pitting potential. Samples preconditioned in the presence of RB have shown a similar pitting potential to the samples preconditioned without flavins. However, it was observed that the pit nucleation was greatly influenced by the presence of flavins, where less but larger and deeper pits were observed in comparison to the samples polarized in the absence of flavins. Overall, the results highlight the large parameter set controlling corrosion properties of passive films and demonstrate that to achieve a profound understanding of the mechanisms of MIC, the possible effects of the redox-active biomolecules have to be considered, as they may play an important role in the corrosion susceptibility of steel surfaces.

ACKNOWLEDGMENTS

Authors gratefully acknowledge Christiane Weimann (BAM Berlin) for technical support at the SEM and Matthias Dimper for the plasma optical emission spectrometry results. Open access funding enabled and organized by Projekt DEAL.

CONFLICT OF INTERESTS

The authors declare that there are no conflict of interests.

AUTHOR CONTRIBUTIONS

Formal analysis, investigation, methodology, writing original draft; writing review and editing: Nina Wurzler. *Investigation, writing review and editing*: Oded Sobol. *Investigation, writing review and editing*: Korinna Altmann. *Methodology, writing review and editing*: Jörg Radnik. *Conceptualization, supervision, writing review and editing*: Ozlem Ozcan.

DATA AVAILABILITY STATEMENT

The data that support the findings of this study are available from the corresponding author upon reasonable request.

ORCID

Ozlem Ozcan http://orcid.org/0000-0002-7457-4985

REFERENCES

[1] C. O. A. Olsson, D. Landolt, *Electrochim. Acta* **2003**, *48*, 1093.
[2] J. J. de Damborenea, A. B. Cristobal, M. A. Arenas, V. Lopez, A. Conde, *Mater. Lett.* **2007**, *61*, 821.
[3] L. Freire, M. A. Catarino, M. I. Godinho, M. J. Ferreira, M. G. S. Ferreira, A. M. P. Simoes, M. F. Montemor, *Cem. Concr. Compos.* **2012**, *34*, 1075.
[4] A. Seyeux, S. Zanna, A. Allion, P. Marcus, *Corros. Sci.* **2015**, *91*, 352.
[5] J. J. Kim, Y. M. Young, *Int. J. Electrochem. Sci.* **2013**, *8*, 11847.
[6] P. Y. Zhang, D. K. Xu, Y. C. Li, K. Yang, T. Y. Gu, *Bioelectrochemistry* **2015**, *101*, 14.
[7] E. Marsili, D. B. Baron, I. D. Shikhare, D. Coursolle, J. A. Gralnick, D. R. Bond, *Proc. Natl. Acad. Sci. U. S. A.* **2008**, *105*, 3968.
[8] J. K. Fredrickson, M. F. Romine, A. S. Beliaev, J. M. Auchtung, M. E. Driscoll, T. S. Gardner, K. H. Nealson, A. L. Osterman, G. Pinchuk, J. L. Reed, D. A. Rodionov, J. L. M. Rodrigues, D. A. Saffarini, M. H. Serres, A. M. Spormann, I. B. Zhulin, J. M. Tiedje, *Nat. Rev. Microbiol.* **2008**, *6*, 592.
[9] D. R. Lovley, *Curr. Opin. Biotechnol.* **2008**, *19*, 564.
[10] A. A. Carmona-Martinez, F. Harnisch, U. Kuhlicke, T. R. Neu, U. Schroder, *Bioelectrochemistry* **2013**, *93*, 23.
[11] N. Wurzler, J. D. Schutter, R. Wagner, M. Dimper, D. Lützenkirchen-Hecht, O. Ozcan, *Electrochem. Commun.* **2020**, *112*, 106673.
[12] Y. A. Gorby, S. Yanina, J. S. McLean, K. M. Rosso, D. Moyles, A. Dohnalkova, T. J. Beveridge, I. S. Chang, B. H. Kim, K. S. Kim, D. E. Culley, S. B. Reed, M. F. Romine,

D. A. Saffarini, E. A. Hill, L. Shi, D. A. Elias, D. W. Kennedy, G. Pinchuk, K. Watanabe, S. Ishii, B. Logan, K. H. Nealson, J. K. Fredrickson, *Proc. Natl. Acad. Sci. U. S. A.* **2006**, *103*, 11358.
[13] C. R. Myers, J. M. Myers, *J. Bacteriol.* **1992**, *174*, 3429.
[14] A. Kappler, M. Benz, B. Schink, A. Brune, *FEMS Microbiol. Ecol.* **2004**, *47*, 85.
[15] R. Li, J. M. Tiedje, C. C. Chiu, R. M. Worden, *Environ. Sci. Technol.* **2012**, *46*, 2813.
[16] P. Bianco, J. Haladjian, A. Manjaoui, M. Bruschi, *Electrochim. Acta* **1988**, *33*, 745.
[17] M. Abdelsalam, P. N. Bartlett, A. E. Russell, J. J. Baumberg, E. J. Calvo, N. G. Tognalli, A. Fainstein, *Langmuir* **2008**, *24*, 7018.
[18] H. Liu, S. Matsuda, K. Hashimoto, S. Nakanishi, *ChemSusChem* **2012**, *5*, 1054.
[19] H. von Canstein, J. Ogawa, S. Shimizu, J. R. Lloyd, *Appl. Environ. Microbiol.* **2008**, *74*, 615.
[20] C. Hubschmid, D. Landolt, H. J. Mathieu, *Fresenius' J. Anal. Chem.* **1995**, *353*, 234.
[21] I. Mora-Seró, F. Fabregat-Santiago, B. Denier, J. Bisquert, R. Tena-Zaera, J. Elias, C. Lévy-Clément, *Appl. Phys. Lett.* **2006**, *89*, 203117.
[22] O. Ozcan, K. Pohl, P. Keil, G. Grundmeier, *Electrochem. Commun.* **2011**, *13*, 837.
[23] K. Azumi, T. Ohtsuka, N. Sato, *Trans. Jpn. Inst. Met.* **1986**, *27*, 382.
[24] K. Azumi, T. Ohtsuka, N. Sato, *J. Electrochem. Soc.* **1987**, *134*, 1352.
[25] E. Devito, P. Marcus, *Surf. Interface Anal.* **1992**, *19*, 403.
[26] N. E. Hakiki, M. D. Belo, A. M. P. Simoes, M. G. S. Ferreira, *J. Electrochem. Soc.* **1998**, *145*, 3821.
[27] F. Fattah-Alhosseini, M. M. Khalvan, *J. Adv. Mater. Process.* **2013**, *2*, 15.
[28] D.-S. Kong, S.-H. Chen, C. Wang, W. Yang, *Corros. Sci.* **2003**, *45*, 747.
[29] N. Sato, *Corros. Sci.* **1990**, *31*, 1.

SUPPORTING INFORMATION

Additional Supporting Information may be found online in the supporting information tab for this article.

How to cite this article: Wurzler N, Sobol O, Altmann K, Radnik J, Ozcan O. Preconditioning of AISI 304 stainless steel surfaces in the presence of flavins—Part I: Effect on surface chemistry and corrosion behavior. *Materials and Corrosion*. 2021;72:974–982. https://doi.org/10.1002/maco.202012191